Environment International 169 (2022) 107505

Contents lists available at ScienceDirect

Environment International

journal homepage: www.elsevier.com/locate/envint

Full length article

Development and calibration of a modifiable passive sampler for monitoring atmospheric tritiated water vapor in different environments

Bin Feng [a,b], Georg Steinhauser [a,c], Weihai Zhuo [b], Zhiling Li [b], Yupeng Yao [b], Tobias Blenke [a], Chao Zhao [d], Franz Renz [e], Bo Chen [b,*]

[a] Institute of Radioecology and Radiation Protection, Leibniz Universität Hannover, 30419 Hannover, Germany
[b] Institute of Radiation Medicine, Fudan University, Shanghai 200032, China
[c] TU Wien, Institute of Applied Synthetic Chemistry & TRIGA Center Atominstitut, 1060 Vienna, Austria
[d] Shanghai Institute of Measurement and Testing Technology, Shanghai 201203, China
[e] Institute of Inorganic Chemistry, Leibniz Universität Hannover, 30167 Hannover, Germany

ARTICLE INFO

Handling Editor: Adrian Covaci

Keywords:
Tritium
Passive sampler
Atmospheric monitoring
Field calibration
Radiation protection
Nuclear facilities

ABSTRACT

Anthropogenic release of tritium from nuclear facilities is expected to increase significantly in the coming decades, which may cause radiation exposure to humans through the contamination of water and food chains. It is necessary and urgent to acquire detailed information about tritium in various environments for studying its behavior and assessing the potential radiation risk. In the atmosphere, although the passive sampling technique provides a low-cost and convenient way to characterize the dynamics of tritiated water vapor (HTO), a single, simple sampler configuration makes it difficult to collect sufficient and representative samples within the expected period from different environments. In this study, we systematically studied the impacts of sampler configurations on sampling performance and proposed a modifiable sampler design by scaling sampler geometry and adjusting absorbent to achieve different monitoring demands. The samplers were subsequently deployed at five sites in China and Germany for the field calibration and the measured results exhibited a good agreement between the adsorption process obtained in sites corrected with diffusion coefficient and the one calibrated in Shanghai. This suggests the feasibility of predicting sampling performance in the field based on known data. Finally, we developed a strategy for sampler modification and selection in different environments and demonstrated that using easily obtainable environmental data, our sampler can be optimized for any area without any time-consuming preliminary experiments. This work provides a scientific basis for establishing high-resolution atmospheric HTO database and expands the conventional empirical sampler design paradigm by demonstrating the feasibility of using quantitative indices for sampler performance customization.

1. Introduction

As the radioisotope of hydrogen, tritium (^{3}H, $T_{1/2}$ = 12.33 y) is capable of exchanging with stable hydrogen in various environmental components and in turn, poses radiation risk to humans though the contamination of water and food chains (Le Goff et al., 2014, Eyrolle et al., 2018; Nie et al., 2022). Natural production of tritium is mainly governed by nuclear reaction in the upper atmosphere, which forms a dynamic tritium baseline in the environment (Boyer et al., 2009; Feng and Zhuo, 2022). Nuclear weapon tests introduced remarkable amounts of anthropogenic tritium into the stratosphere in the middle 1900s (Cauquoin et al., 2015); the subsequent increase of environmental tritium levels by 2–4 orders of magnitude provided an impressive recognition on tritium contamination (Morgenstern et al., 2010). With the implementation of the Partial Nuclear Test Ban Treaty since 1963, anthropogenic tritium releases are currently dominated by operations of civilian nuclear facilities, such as nuclear power plants and reprocessing plants (Kim et al., 2012; Ko et al., 2017; UNSCEAR, 2017). It has been estimated that the anthropogenic release of tritium will have a significant increase in the coming decades (Nivesse et al., 2021; Nie et al., 2021) due to: (1) rapid construction of numerous nuclear power plants in the world (IAEA, 2022); (2) recent plans to discharge the tritium-contaminated wastewater stored in Fukushima into the Pacific Ocean (Querfeld et al., 2019; Buesseler, 2020; Bezhenar et al., 2021; Zhao

* Corresponding author.
E-mail address: bochenFYS@fudan.edu.cn (B. Chen).

https://doi.org/10.1016/j.envint.2022.107505
Received 6 July 2022; Received in revised form 1 September 2022; Accepted 2 September 2022
Available online 6 September 2022

et al., 2021); (3) ongoing progress in international thermonuclear experiments and fusion power technologies that will process considerable ^{3}H (Nie et al., 2017; Nivesse et al., 2021; Chen et al., 2021). Therefore, it is essential and urgent to have a comprehensive understanding of the occurrence, fate, and exposure risk of tritium in the environment. The acquisition of detailed and reliable dataset on characterizing environmental ^{3}H dynamics is a prerequisite for achieving this goal.

In the atmosphere, tritiated water vapor (HTO) is the dominant form of tritium and has triggered a critical attention by the field of radiation protection owing to its high mobility, long persistence, and radiation threat (Connan et al., 2017; Hirao et al., 2022). Over the last decades, extensive monitoring campaigns have been conducted near nuclear facilities and background sites for recording the dynamics of atmospheric HTO (Akata et al., 2011a; Kamath et al., 2018; Hamlat et al., 2018; Qin et al., 2019). However, routine grab sampling technique is costly and labor-intensive for simultaneous monitoring campaigns in large-scale areas and only provides a snapshot concentration in a short term, resulting in a poor resolution and representativeness in HTO monitoring dataset currently. This impedes our ability to accurately identify anthropogenic ^{3}H emissions and assess their exposure levels and environmental risks. Although continuous sampling devices would largely improve the representativeness and temporal resolution of monitoring data, the relatively high cost and electricity dependence limit their deployment in the field (Uda et al., 2006; Connan et al., 2017; Qin et al., 2018).

Passive sampling has many potential benefits in establishing high-resolution monitoring networks because of its low cost, convenience, and electricity independence (Zhang et al., 2017; Rauert et al., 2018; Hirao and Kakiuchi, 2021). During the deployment, atmospheric HTO are continuously accumulated in the absorbent through molecular diffusion, which allows the measured data to represent an average of concentration dynamics (Feng et al., 2017). Limited by the absorbent capacity, however, only the samples collected during the quasi-linear stage are representative (Zhang et al., 2012a). In this context, an appropriate sampling rate (*SR*, $m^3\ d^{-1}$) is required to match the sampling capacity in a given environment and sampling demand. Moreover, because *SR* would also be influenced by wind, which can lead to an uncontrollable *SR* in the expected period, additional efforts are required to reduce the wind-caused turbulence inside the sampler (Zhang et al., 2013). Previous studies attempted to adjust the samplers' structural configurations for meeting the atmospheric HTO sampling needs in different scenarios (Wood and Workman, 1992; Wood, 1996; Iida et al., 1995; Akata et al., 2011b). However, owing to the lack of quantifiability of the role of the various configuration parameters in sampling performances, the existing samplers typically relies on the designer's experience, which makes it difficult to together meet the requirement of sampling rate and sampling stability in the environments with different climatic characteristics. The issues related to sampling methodology may result in a decrease in the representativeness and reliability of the monitoring results.

In our early work (Feng et al., 2017), the geometry of an HTO sampler was optimized based on computational fluid dynamics (CFD) simulation to improve sampling stability. By now, this sampler has been applied in radiation monitoring networks (Feng et al., 2017) and long-term HTO baseline investigation in mainland China (Feng et al., 2019). However, previous practices showed that the simple adjustment of the opening hole may still be arduous to provide an expected *SR* in different cases. For example, the collected quantity in a dry environment maybe not sufficient for precise tritium measurement even after a deployment of more than two months, while the absorbent may easily reach to the equilibrium in a wet environment. These issues suggest the need to consider different sampler configurations in different environments. Yet, the role of sampler configurations and environmental parameter changes in sampling performance remains unclear, which fundamentally limits the possibility to propose an appropriate sampler design for HTO monitoring in unstudied environments.

The overall aim of this study was therefore to develop a modifiable sampler design with appropriate and stable *SR* for collecting atmospheric HTO from different environments, and in turn to facilitate our understanding of occurrence, fate, and risk of atmospheric tritium by improving the quality of monitoring datasets. For this purpose, we systematically study the sampler configuration (materials and structure) impacts on sampling performance (sampling rate and sampling stability), and present for the first time a modifiable sampler design by scaling the sampler structure and adjusting the absorbent to enable custom modifications of sampler performance for any area. Besides, we conducted field calibration experiments in China and Germany to examine the flexibility and reliability of samplers. Combining the experimental results and our practical experience, we developed a comprehensive strategy for the selection of a passive sampler configuration under different exposure conditions. Our work also hopes to facilitate a shift in the sampler design concept from personal experience to reliance on factual and quantitative parameters.

2. Materials and methods

2.1. Overall consideration of the factors affecting sampling performance

In this study, the initial sampler configuration is based on our previous suspension design (Feng et al., 2017). As shown in Fig. 1, the sampler is assembled with four detachable components, including a bottom lid with opening, diffusion zone, absorption zone, and top lid. A commercially available polymethyl methacrylate (PMMA) tube was adopted to construct the sampler body thanks to its low cost and structural adaptability. A high-density filter membrane was covered upon the bottom opening to avoid insects' entry. The atmospheric water vapor can diffuse through the bottom opening into the sampler during deployment. Inside the sampler, a 200-mesh stainless steel screen was fixed in the bottom of the absorption zone to allow absorbent contact with the incoming air. Hence, the atmospheric water vapor will migrate along the concentration gradient and ultimately accumulate in the absorbent.

During the sampling process, the water vapor uptake in absorbent (m_s) is the function of the deployment time (t), average water vapor concentration in the atmosphere (C), and the equilibrium amount of the absorbent (EA):

$$m_s = EA \bullet \left(1 - e^{-a \bullet C \bullet t}\right) \quad (1)$$

.where a donates the fitting parameter

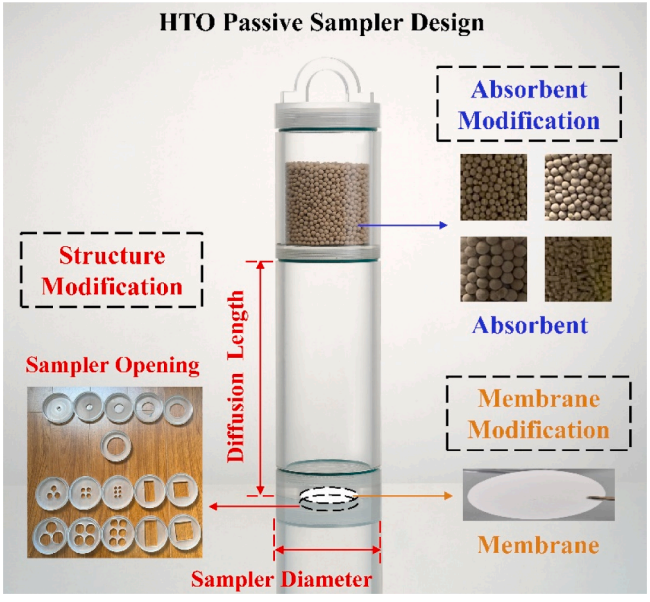

Fig. 1. The configuration of HTO passive sampler used in this study.

related to the absorbent's exposure area, the overall mass transfer coefficient, and the equilibrium amount of the absorbent.

At the initial sampling stage, the uptake (m_s, g) is linearly correlated with the cumulative exposure ($C \times t$, g m^{-3}h), so the linear sampling rate (SR, m_s / ($C \times t$), m^3h^{-1}) is often used as a quantitative index reflecting sampling capacity (Salim and Górecki, 2019). In most scenarios, SR is independent with the expected cumulative exposure because the uptake of general pollution is much lower than the linear load of used absorbent (Zhang et al., 2011; Snow et al., 2021). The formula of one-dimensional Fick's law simplifies SR to be associated only with the exposure area of absorbent and diffusion length (Gerboles et al., 2005). Whereas in our case, the high humidity in the atmosphere and limited equilibrium amount of absorbent together makes the effectiveness of linear sampling process still constrained by the absorbent feature. Therefore, the choice of materials used (i.e., absorbent size and filter membrane type) and the configuration of sampler structure (i.e., opening geometry, diffusion length, and exposure area) were thought as the key factors influencing sampling performance.

2.2. Sampler preparation

A sampler with given configuration (absorbent: 300 g of MS-4 Å; filter: polypropylene filter membrane) and geometric structure (single hole with open diameter, O = 43 mm; diffusion length, H = 200 mm; inner diameter, D = 80 mm) were prepared as the reference for evaluating the effectiveness of modifications.

To investigate the effect of absorbent grain size on sampling rate, different sizes of MS-4 Å (spherical particle: 1–3 mm; 3–5 mm; 5–8 mm; cylindrical particle: 3.2 mm) produced by a commercial company (Shanghai zeolite molecular sieve co., ltd, China) were prepared for the reference samplers. Besides, it was reported that the SR can vary with the amount of loaded absorbent because the absorption process can occur in both the macropores and micropores inside the absorbent (Zhang and Wania, 2012). To investigate the influence of absorbent loading, the MS-4Å (3–5 mm sphere) with the amounts of 100 g, 200 g, and 300 g were prepared in the reference samplers, respectively.

Considering the types of filter membrane may affect sampling rate and sampling stability via controlling the mass transfer resistance at the opening, to assess the role of this variable, three commercial filter membranes including glass filter membrane (Whatman, 1825-047, UK), Supor PES filter membrane (Waters, WAT200538, USA) and mixed cellulose (MC) filter membrane (Advantec, A080A047A, Japan) were used in the reference sampler except for the polypropylene (PP) filter membrane (Delv, China) used in this study. Moreover, additional two kinds of samplers, including a set without filter membrane and the one covered double PP (i.e., PP-PP) filter membranes were also prepared to enrich the mass transfer resistance in filer region.

To learn the role of opening configuration in sampling performance, the reference sampler was equipped with the bottom lids having different opening configurations. Specifically, to study the impact of opening rate on SR, the diameter of single opening was replaced by a batch of single circular openings (O: 13, 23, 33, 51, 60; unit: mm). To investigate if or not SR is mainly governed by opening rate rather than opening shape, we prepared a series of the bottom lids with single rectangular or single square openings. Their opening area or perimeter were set as same as a single circular opening design (O = 60 mm). Besides, we also produced some bottom lids with triple holes, quadruple holes, and hexaploidy holes for studying the role of opening arrangement in sampling performance. Similarly, their accumulated opening area or perimeter were also adjusted to be the same as the one with opening of 60 mm.

The diffusion length is a well-studied parameter in the many passive samplers because it can affect the sampling rate and the sampling stability (Üzmez et al., 2020). To quantitatively evaluate the role of diffusion length in sampling performance, the diffusion tubes with different lengths (H: 50, 100, 150, 250, and 300 mm) were prepared for the reference sampler.

Because of the ideal structural symmetry of cylindrical body and single circle opening in reference sampler, we hypothesize that the SR will vary consequently but the sampling stability under turbulent condition can remain relatively consistent if the sampler structure is scaled by the inner diameter of PMMA tube. To validate this idea, the PMMA tubes with the inner diameter of 60 mm and 100 mm were used for constructing scaled-up sampler (O = 54 mm; H = 250 mm; D = 100 mm) and scaled-down sampler (O = 32 mm; H = 160 mm; D = 60 mm) based on the structural proportions of reference sampler. The bottom lids with the opening diameter of 9.3 mm (D = 60 mm) and 16.3 mm (D = 100 mm) were also prepared. Table S1 (see part 1 in the Supplementary material) summarized the detailed structural parameters of all sampler configurations used in this study. The diffusion length (H, mm) and the ratio (OR) between opening area (OS, $OS = (O/2)^2 \times \pi$, mm^2) and exposure area (S, $S = (D/2)^2 \times \pi$, mm^2) were set as the quantitative indices of sampler structure.

2.3. Exposure experiments in the laboratory

In order to investigate the SR of those prepared samplers, the static water vapor exposure experiments were conducted in an unoccupied room. The temperature and humidity in this room were continuously recorded by a calibrated meteorological logger (ZOGLAB, China) with a temporal resolution of 5 min. During the experiments, as the fluctuations in temperature (23.0 ± 0.5 ℃) and humidity (11.0 ± 1.3 g m^{-3}) were relatively narrow, the exposure conditions were thought relatively consistent across different batches of experiments. To learn the variation in the linear absorption range of the passive sampler loading different amounts of absorbent, the reference sampler and the prepared samplers filled MS-4 Å with 100 g and 200 g were deployed in the room until their adsorption equilibrium. The daily uptake of sampler was measured by an analytical balance (readability: 0.01 g). Combining the quantified uptake and cumulative exposure, the absorption kinetic curve for each sampler was fitted by using equation (1). For other samplers, at least triple replicates were deployed for evaluating sampling rates. Before the deployment, all the samplers were filled with 300 g of the MS-4Å (spherical 3–5 mm) unless otherwise mentioned (i.e., the group with different absorption sizes). In each experiment batch, about 15–20 passive samplers were simultaneously deployed in the room for 5–7 days exposure where the cumulative humidity was approximately 1300 g m^{-3} h.

Exploring the quantitative relationship between sampler configuration and sampling stability was another focus in this study. To assess the sampling stability of all prepared samplers, turbulent water exposure experiments were carried out in above unoccupied room. Twelve alternating current (AC) cooling fans were horizontally fixed on the lab bench countertops to generate twelve similar wind fields. The wind speed was measured by a hot-film anemometer (SMARTSENSOR®, AR866, USA). Two replicate samplers filled with absorbent were vertically fixed to a mobile hanger by S-hooks, while their openings were perpendicular to the wind field's direction. The hanger position was adjusted to a wind speed at the samplers' openings of about 4.0–4.5 m s^{-1}, which was thought to represent wind conditions outside. Similarly, the prepared samplers were deployed in the room for 5–7 days exposure. The turbulent sampling rate was derived from the ratio of sampler uptake to the cumulative humidity at the level of approximately 1300 g m^{-3} h. The sampling stability was evaluated by the ratio between the mean value of sampling rates derived from turbulence conditions (SR_w) and the values obtained in static conditions (SR_s, i.e., SR). The quality assurance and quality control (QA/QC) of experiments were provided in the part 2 of Supplementary Material (Fig. S1-S3, Table S2).

2.4. Field calibration experiments

In addition to wind speed, the spatial and temporal differences in

temperature and atmospheric pressure can also affect the *SR* via controlling the diffusion coefficient (Klánová et al., 2008; Gong et al., 2017). From the viewpoint of making a sampling plan, quantifying the relationship between *SR* and geographic parameters may provide a chance to predict the *SR* in field sites based on known data, which could help to verify whether or not the sampler configuration meets the expected monitoring requirement. Moreover, there is also a need to test the sampling performance and flexibility of the modified samplers in complex field environments. Therefore, the field calibration experiments were conducted at five sites with different geographical and climatologic features, including Shanghai, Haikou, Jiayuguan, and Naqu in China and Hannover in Germany (Fig. 2 and details provided in Table S3). The extensive spans in altitude (9–4515 m), latitude (20.04–52.40 °N), and longitude (9.70–121.47 °E) of these sites cover the majority of meteorological differences among field sites, which allow a wide representation of the calibrated results.

At each site, the reference sampler and the modified sampler with opening diameters of 60 mm were deployed at the position about 1 m above the ground. Considering the significant difference in water vapor exposure at these sites, the up-scaled sampler (No. 35 in Table S1) and down-scaled sampler (No. 33 in Table S1) were set at the dry sites (Jiayuguan and Naqu) and humid site (Haikou), respectively, while both size-scaled sampler were installed in Shanghai site for providing reference curves. Before the deployment, all samplers were filled with 300 g of MS-4 Å (a kind of aluminosilicate), and the bottom were covered by sealed lids to minimize unintended water vapor uptake. The MS-4Å purchased from Shanghai zeolite molecular sieve Co., ltd. (China) and Disidry® Silicagel (Italy) were used in the experiments conducted in China and Germany, respectively. The prepared samplers and modified bottom lids were subsequently sealed in the aluminum foil bag for delivery. The bottom lid was replaced on sites, and the gaining weight of sampler was measured approximately every-three days. The meteorological logger was severed in each site to record the dynamics of temperature and humidity. The ambient wind speed and atmospheric pressure data were derived from the meteorological monitoring station proximal to the experimental site.

3. Results and discussion

3.1. Impacts of the absorbent configuration

Fig. 3a exhibits the absorption kinetic curve of the reference sampler in the static environment. The cumulative exposure concentration for reaching 20 %, 25 %, and 50 % of its *EA* (approximately 64 g in this study) were approximately 3457, 4455, and 10668 g m^{-3} h, respectively, which equals about 10-, 12-, and 30-days field-deployment at a humidity concentration of 15 g m^{-3}. Given the minimum sample volume for tritium measurement using liquid scintillation counting (LSC) method requires 8 mL (corresponding to the minimum detection activity of about 1 BqL^{-1}) (Feng et al., 2020), while it was reported that the absorbent's linear stage is usually within the 25 % of equilibrium amount (Zhang et al., 2012a). This indicates that a 2-weeks averaged atmospheric HTO concentration could be available by the reference sampler. However, a longer deployment might be taken for dry regions to achieve the threshold of analysis. Moreover, given that tritium levels in the low-latitude or coastal regions are typically below 1 BqL^{-1} (Hou, 2018; Anh et al., 2018; Jean-Baptiste et al., 2018; Ducros et al., 2018; Gusyev et al., 2019), a higher analytical volume (>50 mL) is also needed to guarantee measurement precision (Feng et al., 2020). If a linear range <25 % *EA* is still to be considered, a simultaneous deployment of multiple reference samplers is needed for sufficient sample amount with the expected period, which may not only increase the cost of monitoring but also cause inconvenience in samplers' deployment and transport.

Extending the linear range is a convenient way to address this problem. If setting the *SR* of 20 % *EA* as a reference, the *SR* would decrease by about 5 % and 20 % when the uptake reaches the 25 % *EA* and 50 % *EA*, respectively. This may still be an acceptable uncertainty for field monitoring. Additionally, the increase of absorbent loading amount and thus enhancing the equilibrium amount is an alternative option. The absorption kinetic curves for samplers with different absorbent amounts (i.e., 100, 200 and 300 g) are illustrated in Fig. 3b. It shows that their absorption kinetic curves nearly overlap at the linear stages. The ANOVA analysis confirms that the difference in their sampling rate derived at the linear absorption stage is not statistically significant ($P = 0.44$). Since the higher absorbent loading means having a larger volume of internal mesopores and micropores, these results indicate that the absorption process in the linear stage is not dominated by the inner portion of absorbent. Furthermore, the targeted molecule

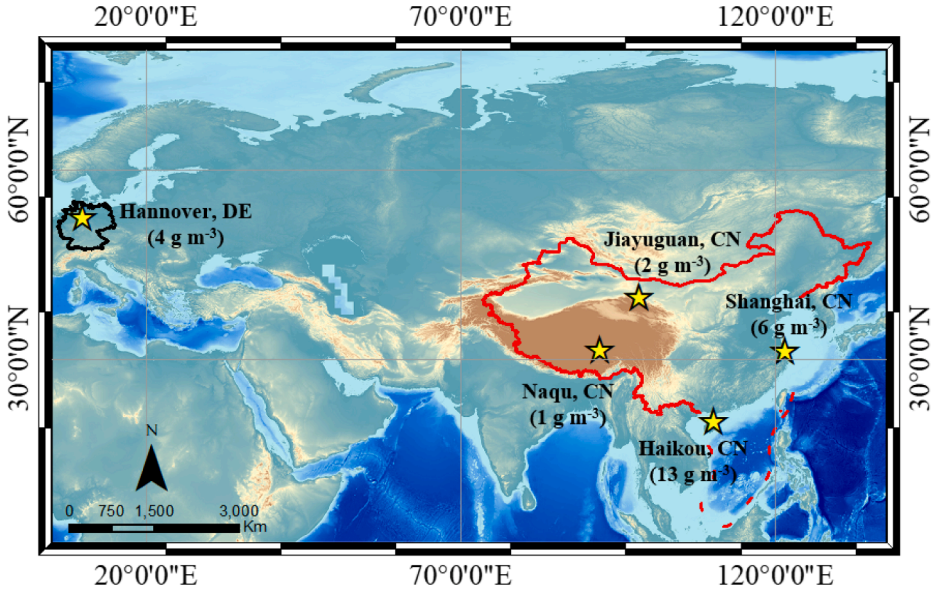

Fig. 2. The locations and humidity conditions in filed calibration sites. The absolute humidity shown in the Figure are the mean value during the deployment periods.

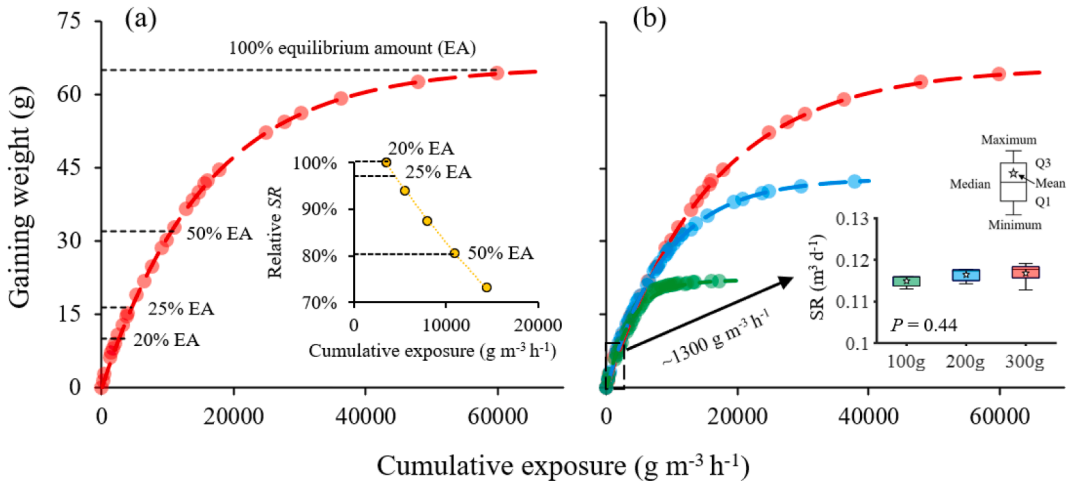

Fig. 3. (a) Absorption kinetic curve for reference sampler and (b)modified samplers with different absorbent amounts.

can also diffuse in the stagnant air layer at the interface of the absorbent surface and air inside the sampler and the macropores between absorbent pellets (Zhang et al., 2011; Snow et al., 2021). However, Fig. 4 shows no statistically significant difference in the *SR* derived from those samplers filled with different grain sizes of MS-4Å, implying that the direct exposure area of the absorbent (i.e., its interface with air) may be a more dominant factor influencing the *SR* during the linear absorption stage.

3.2. Impacts of the filter configuration

Fig. 5a shows the static sampling rates of the samplers using different filter membrane configurations. The difference in these sampling rates was statistically significant (ANOVA, $P < 0.01$). Specifically, the *SR* of the sampler without membrane cover is 0.185 ± 0.012 m^3d^{-1} (mean ± standard deviation), which is ~200 % higher than the configuration having a double-layer PP membrane (0.093 ± 0.004 m^3/d). In comparison, although the difference in *SR* can also be observed in those samplers covered with a single-layer membrane (ANOVA, $P < 0.05$), the variation of these *SR* is relatively narrow, only corresponding to 20 % of the reference *SR* (0.117 ± 0.002 m^3d^{-1}). From the turbulent exposure experiments (Fig. 5b), we note that the sampling stability of the double-layer membrane cover design (SR_w / SR_s = 1.09 ± 0.05, SR_w: derived from turbulent experiment; SR_s: derived from static experiments) is better than that of the non-membrane covered design (SR_w / SR_s = 1.19 ± 0.08), but unexpectedly, the single-layer membrane-covered designs have a slightly poor performance in stability (SR_w / SR_s = 1.25 ± 0.06). Overall, these results reflect the impacts of variation in mass transfer resistance at the bottom opening on the sampling rate and sampling stability. Especially from the double-layer membrane configuration, the

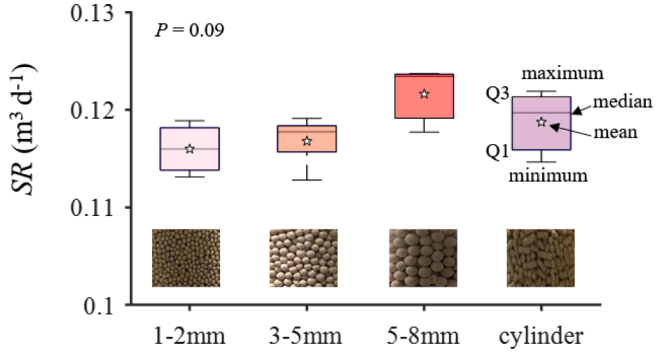

Fig. 4. The influence of grain size of absorbent on sampling rate.

effectiveness of increasing the mass transfer resistance at the bottom opening region in reducing sampling rate and enhancing sampling stability. Nevertheless, the lack of quantifying the characteristic parameters of filter membrane (e.g., pore size distribution, porosity, and pressure drop) limited our ability to further explore the relationship between mass transfer resistance and sampling performance. On the other hand, although our results do not illustrate a significant advantage of using single-layer membrane design in adjusting sampling rate or improving sampling stability, from the viewpoint of field application, having a filter membrane on the bottom opening remains meaningful because it can reduce the risk of absorbent damage and improve the monitoring robustness.

3.3. Impacts of the structure configuration

The *SR* derived from the modified samplers with different opening holes are presented in Fig. 6a-c. A good correlation (Spearman, $r = 0.88$, $P < 0.01$) between opening ratios and *SR* were observed in the sampler configurations either having single circle hole (Fig. 6a) or multi-holes or rectangular opening (Fig. 6b and 6c). Due to the constraint of the sampler inner diameter, we observed a stronger correlation between the sampling rate and the square root of the opening ratio in the fitted model ($R^2 = 0.92$, $P < 0.01$). Moreover, for the samplers assembling the same opening ratio but different shape or hole arrangement, we did not find their sampling rates are different with statistical significance (ANOVA, $P = 0.30$), which indicates the dominant role of the opening ratio in controlling the water vapor being transported into the sampler inside. However, given that the fully symmetrical structure allows the sampler to have the same absorption response to water vapor from different directions, we would suggest using the single-hole bottom lid design.

Diffusion length is another crucial parameter affecting sampling performance. As shown in Fig. 6d, we depict the linear regression relationship between $1/H$ with *SR*, which is consistent well with the trend shown by one-dimensional Fick's model. It should be noted that the *SR* of sampler using a 30 cm diffusion tube only declined by approximately 20 % compared to the configuration using a 5 cm diffusion tube, though their diffusion length varies by 6-fold. Compared to the change in sampling rate by adjusting the opening ratio, the effect of varying diffusion length is relatively limited.

3.4. Quantification of sampler configuration and sampling performance

In order to quantify the samplers' structural configurations and establish the link between these quantified parameters and the corresponding *SR*, a structure-related index (T, $T = (S / H) \times OS^{1/2}$) based on experimental data and theoretical models was proposed. The equivalent

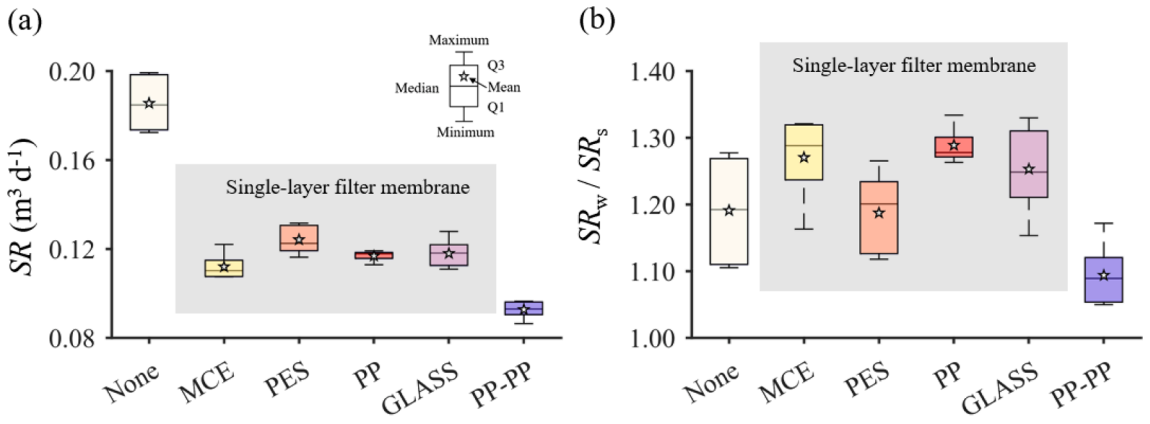

Fig. 5. The influence of membrane filter types on (a) sampling rate and (b) sampling stability. The MCE, PES, PP, and GLASS represent the filter membranes made by mixed cellulose, hydrophilic polyethersulfone, polypropylene, and glass fiber respectively. The PP-PP donate the double polypropylene filter membranes.

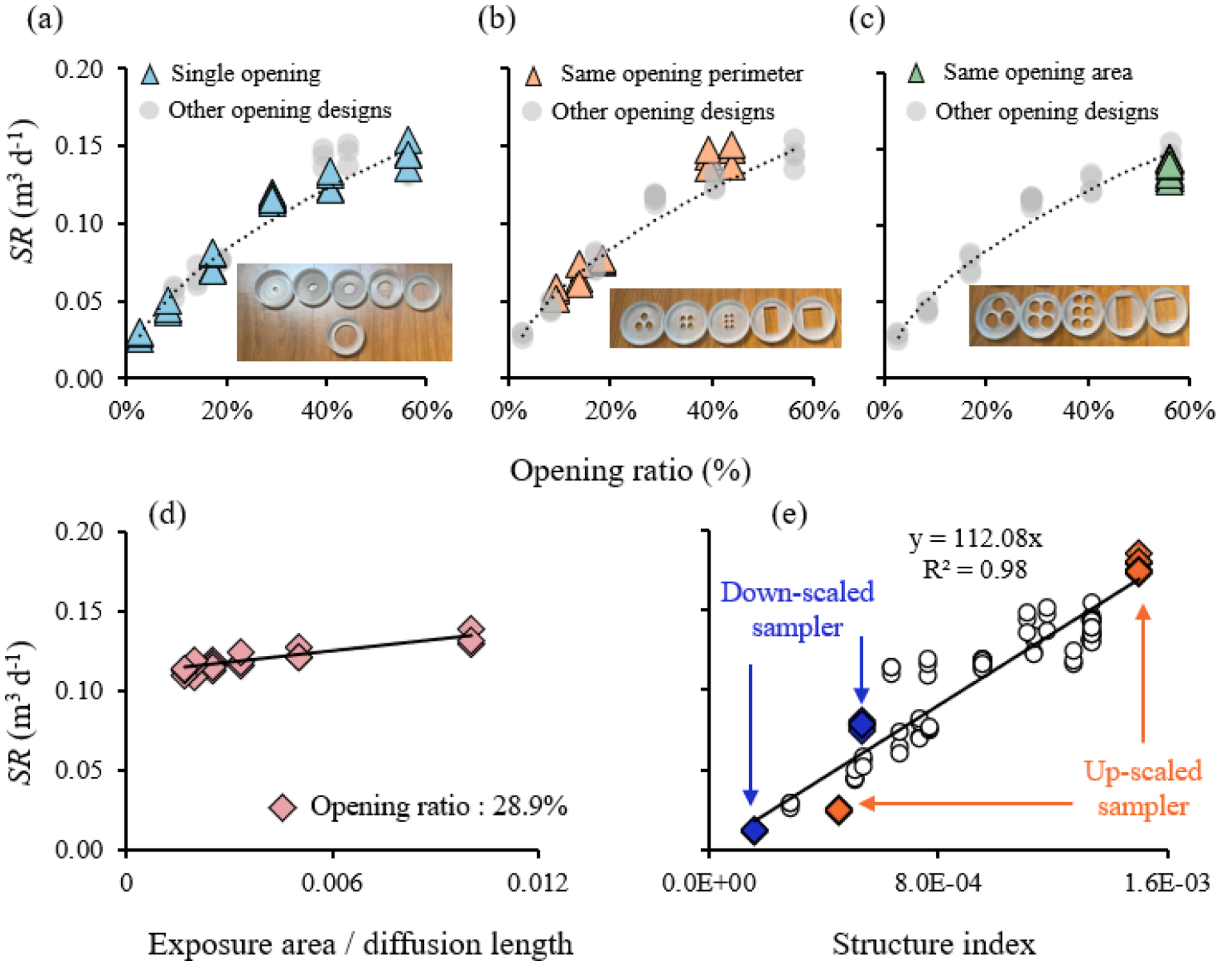

Fig. 6. The variation of sampling rate in different structure configurations of passive sampler. (a) sampler with single opening; (b) sampler with same opening perimeter; (c) sampler with same opening area; (d) sampler with different diffusion length; (e) relationship between structure index and *SR*.

opening length ($OS^{1/2}$, mm) that controls the entry of outside ambient air into the sampler and the exposure area (S, mm^2) / diffusion length (H, mm) ratio that controls the mass transfer resistance within the sampler are considered two independent variables in the mathematical expression of this parameter.

Overall, the Spearman analysis illustrates a high correlation (r = 0.89, $P < 0.01$) between the quantified structure index and *SR*, but the regression analysis shows that *SR* based on the configurations with a diffusion length of 5 cm and 10 cm significantly deviates from the fitting linear model. Such difference could be attributed to the shorter diffusion length resulting in a higher concentration gradient, which exceeds the absorbent's equilibrium capacity at the exposed surface. This phenomenon is consistent with previous CFD results (Feng et al., 2017). If we exclude the data originating from these two sets of designs, a high regression model between *T* and *SR* can be achieved with R^2 of over 0.98 ($P < 0.01$). As shown in Fig. 6e, the regression model demonstrates that

the *SR* would increase by 0.11 m^3/d with every 0.001 increase in *T*. Moreover, the *SR* calculated by the scaled sampler well fits the constraints of this model, suggesting the range of *SR* could be significantly expanded by scaling the sampler size.

From the results of turbulent exposure experiments, we know that the sampling stability is negatively correlated with opening ratio (r = -0.67, $P < 0.01$) and diffusion length (r = -0.72, $P < 0.01$), and such negative correlation remains significant if using the structure index (Fig. 7). This somehow reflects the difficulty of achieving high sampling rate and high sampling stability simultaneously. Nevertheless, there is no statistically significant difference in the SR_w / SR_s values for samplers with the same opening ratio (ANOVA, P = 0.30) despite the great difference in their hole sharp or arrangement. More interestingly, although *SR*s of the up-scaled and down-scaled samplers, respectively, show a clear positive correlation with their structural indices, their SR_w / SR_s remain at the same level.

Several studies attributed the variability in *SR* and sampling stability to the difference in the sampler's mass transfer resistance (Hofschreuder et al., 1999; Bartkow et al., 2005; Zhang et al., 2013). In this study, the mass transfer resistance associated with structural configuration mainly involves two parts: (1) resistance from the air-side boundary (r_a) that is associated with equivalent opening length ($OS^{1/2}$, m); (2) resistance from material diffusion inside sampler (r_d) that is related to the exposure area (S, m^2)/ diffusion length (H, m) ratio. For a quantitative assessment of the impact of turbulent-induced mass transfer resistance change on sampling performance, we estimated the mass transfer resistance of different structural designs at wind speed of 4.5 m s^{-1} and 0.1 m s^{-1} (details provided in the part 4 of Supplementary material). Table 1 listed the mass transfer resistances of all samplers under stable and turbulent environments.

First, the r_a changes in the sampler with a lower equivalent opening length (i.e., the lower opening ratio) would be more significant in different exposure scenarios, implying the air increment into the small opening sampler would be relatively higher in turbulent environments. The CFD simulation (Fig. 8, details provided in the part 5 of Supplementary material) shows that the water vapor concentration gradient inside these small-opening samplers is generally low in the static environment. This implies that the absorbents' surface has not reached its absorption equilibrium status yet. Therefore, the high adsorption efficiency of the small-port sampler for the additional introduced water vapor may be a reason for its relatively poor sampling stability. In contrast, the lower r_a would allow easy air exchange inside and outside the big-opening sampler. A higher water vapor concentration gradient inside these samplers also suggests their absorbents' surface is relatively closer to the equilibrium (Fig. 8b). As a result, above two factors limit the *SR* change of big-opening samplers in turbulent environments. Besides, for the samplers with a same opening ratio, the calculation displays their same air-side mass transfer resistance changes though the holes' shape or arrangement is different, which may explain why they have similar stability performance. Note, due to the limited number of opening holes presented in this work, we did not consider the interaction between holes so that such explanation should not be over-extrapolated. In summary, our findings demonstrate that increasing opening ratio would be helpful for improving sampling stability.

Table 1
The resistance variations of each sampler under wind speed of 0.1 and 4.5 m s^{-1}.

Sample ID	Resistance from air boundary (r_a)		Resistance from diffusion (r_d)	Changes of mass transfer resistance ($r_{a\text{-}0.1}$-$r_{a\text{-}4.5}$)/r_d
	Wind = 0.1 m s^{-1}	Wind = 4.5 m s^{-1}		
1	2.90	0.43	39.79	6.2 %
12	31.74	4.73	39.79	67.9 %
13	10.14	1.51	39.79	21.7 %
14	4.93	0.73	39.79	10.5 %
15	2.06	0.31	39.79	4.4 %
16	1.49	0.22	39.79	3.2 %
17	1.49	0.22	39.79	3.2 %
18	1.90	0.28	39.79	4.1 %
19	1.49	0.22	39.79	3.2 %
20	2.14	0.32	39.79	4.6 %
21	4.47	0.67	39.79	9.6 %
22	5.96	0.89	39.79	12.7 %
23	8.94	1.33	39.79	19.1 %
24	1.49	0.22	39.79	3.2 %
25	1.49	0.22	39.79	3.2 %
26	1.49	0.22	39.79	3.2 %
27	2.90	0.43	9.95	24.8 %
28	2.90	0.43	19.89	12.4 %
29	2.90	0.43	29.84	8.3 %
30	2.90	0.43	49.74	5.0 %
31	2.90	0.43	59.68	4.1 %
33	4.54	0.68	53.05	7.3 %
35	2.06	0.31	31.83	5.5 %

3.5. Kinetic absorption curves calibrated in different environments

Fig. 9a-d shows the calibrated kinetic absorption curves for passive samplers at five sites. Overall, good correlations between the cumulative water vapor exposure and absorbent's gaining weight can be observed in all cases. Under the same gaining weight conditions, there is a remarkable difference in the required cumulative exposure for different sampler designs, which emphasizes the need to select appropriate

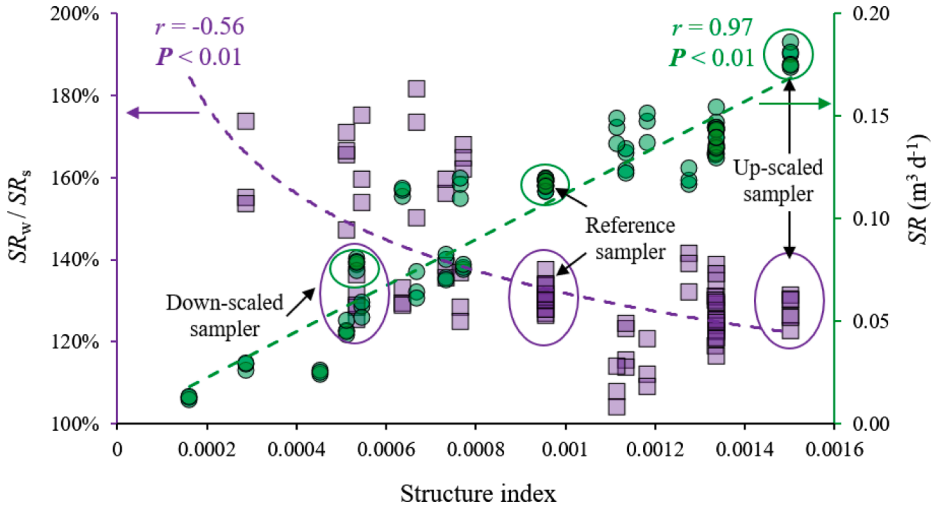

Fig. 7. The role of samplers' design in sampling performance.

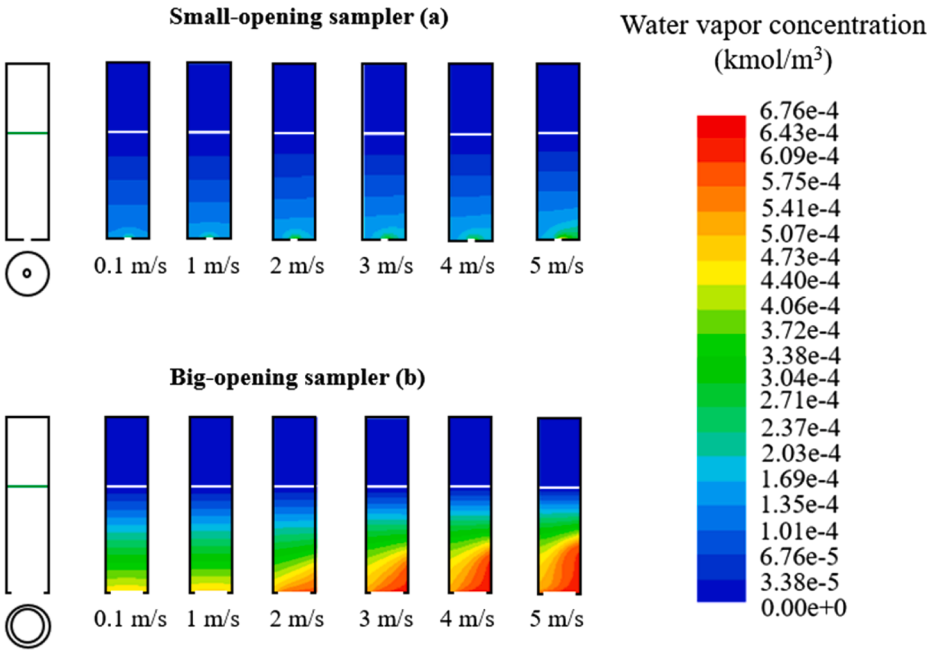

Fig. 8. Water vapor concentration gradient inside the small-opening sampler (a, OR = 14.4 %) and big-opening sampler (b, OR = 66.5 %) under the wind speed varied from 0.1 m s^{-1} to 5 m s^{-1}.As total mass transfer coefficient is the reciprocal of the total mass transfer resistance (i.e., $r_a + r_d$ in this study), increasing the resistance from material diffusion inside sampler (r_d) will somehow dilute the effect of r_a change, which benefit the improvement of sampling stability. Through statistical analysis, we find a strong correlation (r = 0.79, $P < 0.01$) between the sampling stability and r_a/r_d ratio changes (Table 1), further supporting above interpretation. Furthermore, the range in changes of r_a/r_d is very narrow (only 1.8 %) between size-scaled samplers and reference samplers, which well explains why the scaled sampler can maintain sampling stability like reference sampler. For future cylindrical sampler design, we suggest increasing the total mass transfer resistance (e.g., enhancing the diffusion length) for designs where the theoretical estimate of the ratio change in r_a/r_d is higher than 7 %, and then scale the sampler structure to adjust the SR. This logic could also apply to the design of other environmental contaminant samplers.

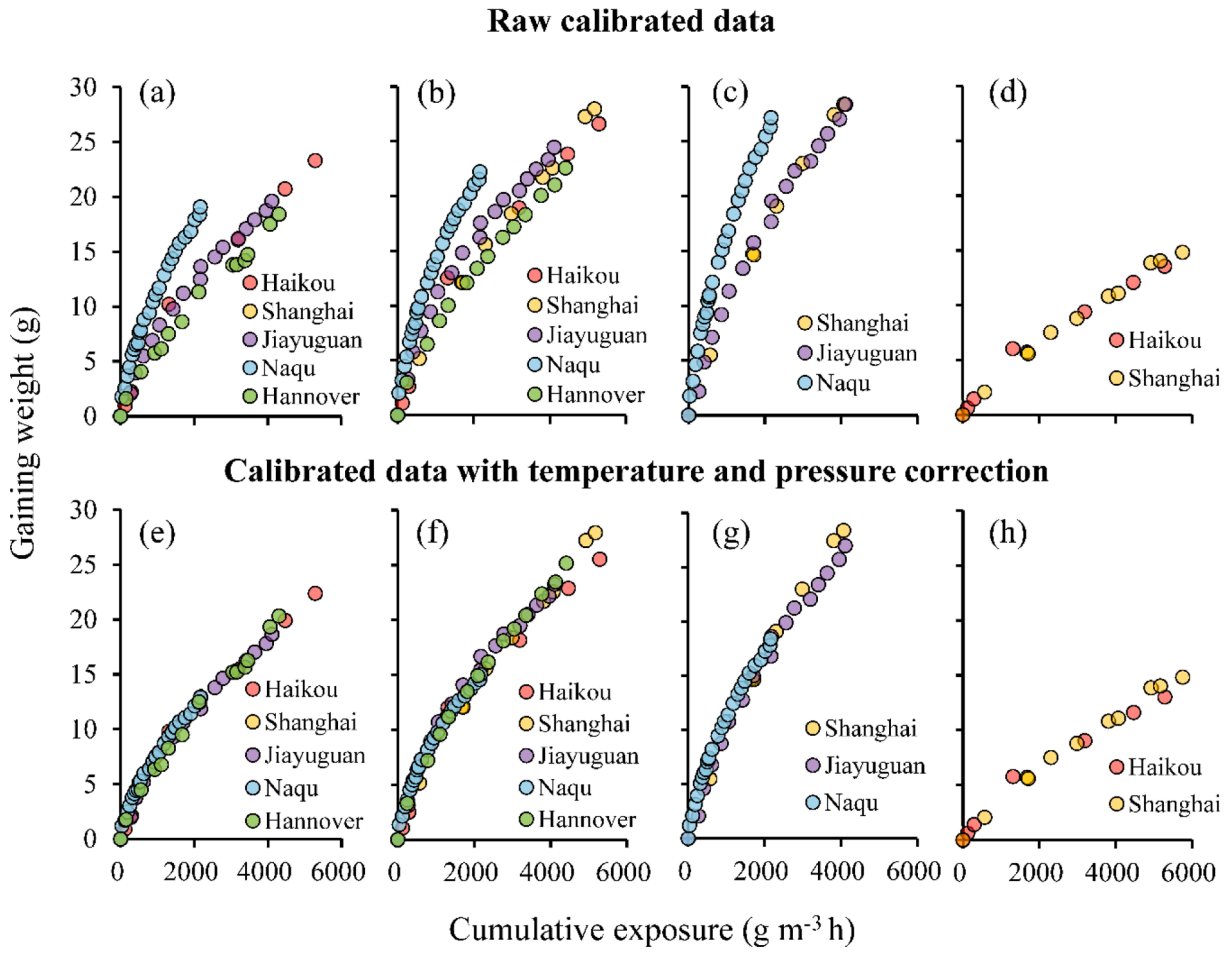

Fig. 9. The calibrated absorption kinetic curves at four field sites. The symbols represent reference sampler (a, e), the samplers with opening diameters of 60 mm (b, f), up-scaled sampler (c, g) and down-scaled sampler (d, h), respectively.

samplers for collecting atmospheric water vapor in different environments. However, we also note a considerable difference in kinetic absorption curves calibrated from different sites despite having the same sampler configuration. To illustrate the difference more quantitatively, we used the nonlinear interpolation in all calibrated kinetic absorption curves for estimating the water uptakes of various passive samplers under a cumulative exposure of 2000 g m^{-3}h. The calculations showed that the coefficients of variation (*CV*, standard deviation/mean) for the reference sampler, modified sampler (D = 60 mm), and up-scaled sampler were about 29 %, 27 %, and 28 % among calibrated sites, respectively. In particular, the water uptakes of the three samplers at the Naqu site in the Tibet region (highland climate) were approximately 49 %, 43 %, and 32 % higher than the mean values of five sites under this given cumulative exposure.

According to the definition of Fick's diffusion law, the linear sampling rate not only depends on sampler's configuration but also is associated with the diffusion coefficient. Given that the chemical's diffusion coefficient in air (D_a, m^2 s^{-1}) is proportional to the exponential power of temperature ($T^{1.75}$, K) and is inversely proportional to the atmospheric pressure (P, kPa) in local (Klánová et al., 2008; Gong et al., 2017), we presumed the higher uptakes observed in Naqu related to its lower atmospheric pressure. To test this hypothesis, all uptake data measured under the linear absorption stage were all corrected by the normalized diffusion coefficient factor (J, dimensionless), which can be calculated by the following equation:

$J = \frac{T_c^{1.75}}{P_c} \times \frac{P_r}{T_r^{1.75}}$ (2).where the T_c and P_c represent the mean value of temperature and atmospheric pressure at the calibration sites during their linear exposure; the T_r and P_r donate above meteorological parameters at shanghai, which is considered the reference site.

Fig. 9e-h presents the corrected absorption kinetic curves of different sampler configurations at five calibration sites. Interestingly, almost perfect overlap can be seen between these adsorption kinetic curves after implementing the diffusion coefficient correction. The coefficients of variation for the reference sampler, modified sampler (D = 60 mm), up-scaled sampler declined to 9 %, 10 %, and 6 % among calibrated sites, respectively. This indicates the difference in meteorological parameters is the key driver causing the diverse response of passive samplers' uptake to cumulative water vapor exposure in different environments. Moreover, this also implies the feasibility of predicting the adsorption process in a given environment by combining the laboratory-calibrated absorption kinetic curves and diffusion coefficient correction based on local meteorological data. Although the mean wind speed records show great differences in five sites, the narrow range between their uptake at 30 % of equilibrium amount may explained by the reason that the absorption process has gradually shifted from the surface layer to the internal mesopores at this stage, resulting in the promotion effect of turbulent-induced mass transfer resistance decline to be not as significant as that in the beginning.

3.6. Strategy for sampler modification and selection

A successful sampler configuration often depends on its ability to achieve the expected monitoring goal, i.e., providing sufficient and representative samples for further analysis. For atmospheric HTO monitoring, the accuracy of tritium determination varies greatly among different monitoring purposes, resulting in a variable need for the collected sample volume. As the atmospheric tritium levels near nuclear facilities are relatively higher than baseline, the use of a conventional LSC method (8 mL water sample in 20 mL counting vial) without additional processing would be sensitive enough for most of the cases (Hou, 2018). In contrast, because the levels of atmospheric tritium are typically lower than 1 BqL^{-1} in coastal and low-latitude regions, a precise measurement often requires a combination of longer counting time and larger sample volume (50 mL water sample in 100 mL counting vial) (Feng et al., 2020; Feng and Zhuo, 2022). Besides, compared to other atmospheric pollutants, as environmental humidity has high temporal and spatial variability, the selection of sampler configuration should comprehensively consider both sample demand and sampling capacity in a specific environment. Furthermore, the field flexibility and deployment convenience should also be considered because passive samplers need to be installed in remote sites sometimes. In views of the above demand, a sampler selection strategy for collecting atmospheric HTO vapor in different environments was proposed in this study.

As shown in Fig. 10, the strategy includes four steps for modifying a passive sampler. First, we use environmental information (i.e., temperature, humidity, atmospheric pressure) and monitoring purposes to estimate the cumulative water vapor exposure, corrected diffusion coefficient (J), and required sample amount (m_1, g). Assuming there is an available absorption kinetic curve in a calibration site, we can thus calculate the collected amount under the given exposure (m_2, g) and estimate the required sample amount in this site (m_3, g) based on m_1/J. Hence, the scaling factor can be derived from the ratio of m_3/m_2 that also equals the ratio of surface exposure area between modified sampler and calibrated sampler. However, the practical size of the inner diameter still needs to be slightly adjusted according to the available tube in market. Ultimately, the corresponding diffusion length and open size could be determined by the scaling factor and the used inner diameter. In addition, because of the regional adaptability of the modified sampler, it should be also emphasized that careful consideration needs to be given to whether or not it is worthwhile to prepare a specific sampler for the area adjacent to the selected monitoring site based on the monitoring plans and modification costs.

In terms of the material use, the absorbent amount to be filled in sampler is also associated with the required sample volume. If the samplers are deployed in the vicinity of nuclear facilities, the loading of about 300 g dried MS-4 Å could meet the requirements of the conventional analysis procedure. While if the monitoring campaigns are organized in those low tritium regions, the demand for linear absorption of over 50 g water vapor would lead to a higher absorbent amount use, and in turn, a longer adsorbent loading zone. In case that samplers are planned to be placed in high humidity region for the long-term, the down-scaled design may lead to a too-long sampler length, which will pose a challenge for sampler installation and transport. A potential solution is to add the thickness of the filter membrane in the appropriate size sampler to enhance the mass transfer resistance. Another approach is to replace the liquid scintillation counter with ^{3}He mass spectrometry for tritium determination. In the ^{3}He ingrowth method, a detection limit of 0.04 BqL^{-1} can be achieved by only using a 20 g water sample (Jean-Baptiste et al., 2010), and the use of 300 g of absorbent would suffice.

4. Conclusion

For high-resolution monitoring data, the time-integrated monitoring technology based on passive samplers is a cost-effective tool that has been applied widely in the monitoring networks of various pollutants. However, the spatial and temporal fluctuation of environmental contaminants and the inherent detection limits of analytical instruments make it challenging to access detailed monitoring information by using a single, simple HTO sampler configuration. In this work, we combined the laboratory experiments, theoretical calculation/simulation, and field calibrations together to systematically exhibit the quantitative impacts of changing HTO sampler configurations (structure and material) on sampling performance (sampling rate and stability) and proposed a specific measure to achieve an appropriate and stable *SR* via scaling the sampler structure and adjusting absorbent. It provides a clear strategy to answer how to reasonably select sampler configuration in different environments. We could demonstrate that using easily obtainable environmental data, this type of sampler can be optimized for any area without any time-consuming preliminary experiments.

From the perspective of radiation protection, our work provides a convenient and affordable way forward of improving our capacity to

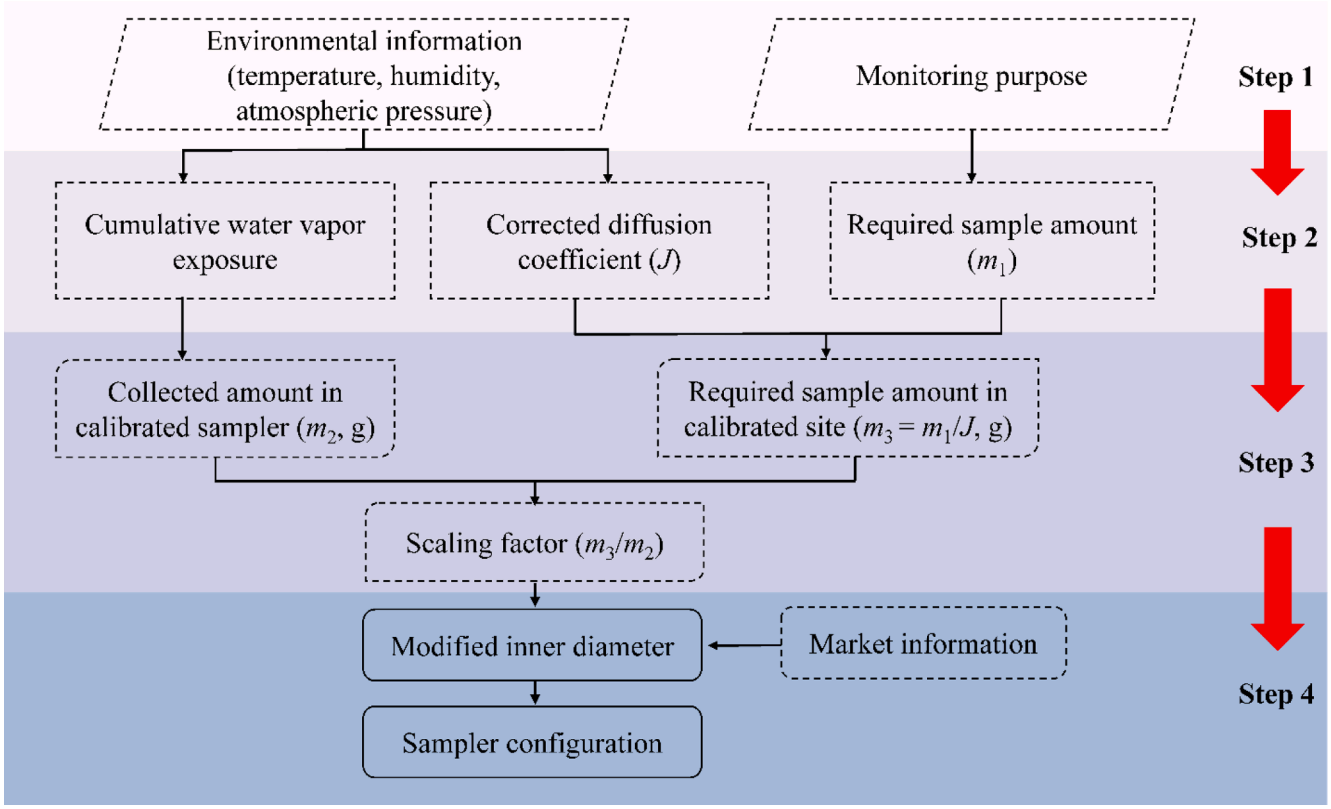

Fig. 10. The sampler modification and selection strategies for different environments.

obtain a tritium dataset with high spatial and temporal resolution. Especially with numerous nuclear power plants currently being constructed around the world and tritium contaminated wastewater in Fukushima are expected to be discharged into the Pacific Ocean, having detailed tritium dynamics would benefit downstream exposure risk assessment and future regulation policymaking. Besides, as the influence of "bomb tritium" has been almost negligible in recent, the natural fluctuations of HTO may influence the identification of anthropogenic tritium source; while the environmental tritium inventory may get back to a relatively high level in the near future (Feng et al., 2019). Therefore, our work also provides a flexible tool to investigate the real tritium baseline in the atmosphere in such a golden window, which will be an important reference for future tritium contamination control. Furthermore, we expanded the traditional way of designing passive sampler based on experience, and demonstrated the feasibility of using multiple quantitative indices, including describing sampler structural configurations and assessing sampler performance, to accomplish a science-based sampler modification. The conclusions and suggestions presented in this work would be informative for designing or modifying passive samplers used in other environmental pollutants monitoring.

CRediT authorship contribution statement

Bin Feng: Conceptualization, Methodology, Validation, Formal analysis, Investigation, Writing – original draft, Visualization. **Georg Steinhauser:** Resources, Writing – review & editing, Supervision. **Weihai Zhuo:** Resources, Writing – review & editing, Supervision. **Zhiling Li:** Investigation, Formal analysis. **Yupeng Yao:** Investigation, Formal analysis. **Tobias Blenke:** Investigation, Formal analysis. **Chao Zhao:** Investigation, Funding acquisition. **Franz Renz:** Writing – review & editing. **Bo Chen:** Writing – review & editing, Project administration, Funding acquisition.

Declaration of Competing Interest

The authors declare that they have no known competing financial interests or personal relationships that could have appeared to influence the work reported in this paper.

Data availability

Data will be made available on request.

Acknowledgement

This work was supported by the National Natural Science Foundation of China (Grant No.11375048), Shanghai Rising-Star Program (No. 19QB1404900), and Science and Technology Program of the Shanghai Municipal Administration for Market Regulation (No. 2021-06). B. Feng is especially grateful for the Postdoctoral Fellowship supported by Alexander von Humboldt Foundation. All authors also appreciate our collaborators (Mr. Mingxing Duan, Mr. Weile Hu, and Mr. Min Zhou) for their assistance in field calibration experiments and Dr. Yining He (Ninth People's Hospital, Shanghai Jiao Tong University School of Medicine) for her assistance in statistical analysis.

References

Akata, N., Kakiuchi, H., Shima, N., Iyogi, T., Momoshima, N., Hisamatsu, S., 2011a. Tritium concentrations in the atmospheric environment at Rokkasho, Japan before the final testing of the spent nuclear fuel reprocessing plant. J. Environ. Radioact. 102, 837–842. https://doi.org/10.1016/j.jenvrad.2011.05.005.

Akata, N., Kakiuchi, H., Kanno, K., Shima, N., Hisamatsu, S., 2011b. Determination of the atmospheric hto concentration around the nuclear fuel reprocessing plant in Rokkasho by using a passive type sampler. Fusion Sci. Technol. 60, 1292–1295. https://doi.org/10.13182/FST11-A12667.

Anh, H.L., Anh, V.T., Giap, T.V., Hong Thinh, N.T., Minh, T.K., Hoai, V., 2018. Monitoring of tritium concentration in Hanoi's precipitation from 2011 to 2016. J. Environ. Radioact. 192, 143–149. https://doi.org/10.1016/j.jenvrad.2018.06.009.

Bartkow, M.E., Booij, K., Kennedy, K.E., Müller, J.F., Hawker, D.W., 2005. Passive air sampling theory for semivolatile organic compounds. Chemosphere 60, 170–176. https://doi.org/10.1016/j.chemosphere.2004.12.033.

Bezhenar, R., Takata, H., de With, G., Maderich, V., 2021. Planned release of contaminated water from the Fukushima storage tanks into the ocean: Simulation scenarios of radiological impact for aquatic biota and human from seafood consumption. Mar. Pollut. Bull. 173, 112969 https://doi.org/10.1016/j.marpolbul.2021.112969.

Boyer, C., Vichot, L., Fromm, M., Losset, Y., Tatin-Froux, F., Guétat, P., Badot, P.M., 2009. Tritium in plants: A review of current knowledge. Environ. Exp. Bot. 67, 34–51. https://doi.org/10.1016/j.envexpbot.2009.06.008.

Buesseler, K.O., 2020. Opening the floodgates at Fukushima. Science 369 (6504), 621–622. https://doi.org/10.1126/science.abc1507.

Cauquoin, A., Jean-Baptiste, P., Risi, C., Fourré, E., Stenni, B., Landais, A., 2015. The global distribution of natural tritium in precipitation simulated with an atmospheric general circulation model and comparison with observations. Earth Planet. Sci. Lett. 427, 160–170. https://doi.org/10.1016/j.epsl.2015.06.043.

Chen, Z., Lai, C., Li, Y., Cheng, S., Yang, Y., Peng, S., 2021. A planar-type ionization chamber for tritium surface contamination measurements in fusion facility. Fusion Eng. Des. 165 https://doi.org/10.1016/j.fusengdes.2021.112258.

Connan, O., Hébert, D., Solier, L., Maro, D., Pellerin, G., Voiseux, C., Lamotte, M., Laguionie, P., 2017. Atmospheric tritium concentrations under influence of AREVA NC La Hague reprocessing plant (France) and background levels. J. Environ. Radioact. 177, 184–193. https://doi.org/10.1016/j.jenvrad.2017.06.015.

Ducros, L., Eyrolle, F., Vedova, C.D., Charmasson, S., Leblanc, M., Mayer, A., Babic, M., Antonelli, C., Mourier, D., Giner, F., 2018. Tritium in river waters from French Mediterranean catchments: background levels and variability. Sci. Total Environ. 612, 672–682. https://doi.org/10.1016/j.scitotenv.2017.08.026.

Eyrolle, F., Ducros, L., Le Dizès, S., Beaugelin-Seiller, K., Charmasson, S., Boyer, P., Cossonnet, C., 2018. An updated review on tritium in the environment. J. Environ. Radioact. 181, 128–137. https://doi.org/10.1016/j.jenvrad.2017.11.001.

Feng, B., Chen, B., Zhuo, W., Zhang, W., 2017. A new passive sampler for collecting atmospheric tritiated water vapor. Atmos. Environ. 154, 308–317. https://doi.org/10.1016/j.atmosenv.2017.01.035.

Feng, B., Chen, B., Zhuo, W., Chen, Q., Zhang, Y., Zhang, W., 2019. Seasonal and spatial distribution of atmospheric tritiated water vapor in Mainland China. Environ. Sci. Technol. 53, 14175–14185. https://doi.org/10.1021/acs.est.9b03855.

Feng, B., Chen, B., Zhao, C., He, L., Tang, F., Zhuo, W., 2020. Application of a liquid scintillation system with 100-ml counting vials for environmental tritium determination: procedure optimization, performance test, and uncertainty analysis. J. Environ. Radioact. 225, 106427 https://doi.org/10.1016/j.jenvrad.2020.106427.

Feng, B., Zhuo, W., 2022. Levels and behavior of environmental tritium in East Asia. Nucl. Sci. Tech. 33, 86. https://doi.org/10.1007/s41365-022-01073-3.

Gerboles, M., Buzica, D., Amantini, L., 2005. Modification of the Palmes diffusion tube and semi-empirical modelling of the uptake rate for monitoring nitrogen dioxide. Atmos. Environ. 39, 2579–2592. https://doi.org/10.1016/j.atmosenv.2005.01.012.

Gong, P., Wang, X., Liu, X., Wania, F., 2017. Field Calibration of XAD-based passive air sampler on the Tibetan Plateau: wind influence and configuration improvement. Environ. Sci. Technol. 51, 5642–5649. https://doi.org/10.1021/acs.est.7b01029.

Gusyev, M.A., Morgenstern, U., Nishihara, T., Hayashi, T., Akata, N., Ichiyanagi, K., Sugimoto, A., Hasegawa, A., Stewart, M.K., 2019. Evaluating anthropogenic and environmental tritium effects using precipitation and Hokkaido snowpack at selected coastal locations in Asia. Sci. Total Environ. 659, 1307–1321. https://doi.org/10.1016/j.scitotenv.2018.12.342.

Hamlat, S., Thompson, P., Rinker, M., St-Amant, N., Pan, P., Peters, K., Dagher, E., Jovanovic, S., Sauvé, K., 2018. Independent environmental monitoring and public dose assessment around the Canadian nuclear power plants. J. Radioanal. Nucl. Chem. 317, 325–335. https://doi.org/10.1007/s10967-018-5903-4.

Hirao, S., Kakiuchi, H., 2021. Investigation of atmospheric tritiated water vapor level around the Fukushima Daiichi nuclear power plant. Fusion Eng. Des. 171, 112556 https://doi.org/10.1016/j.fusengdes.2021.112556.

Hirao, S., Kakiuchi, H., Akata, N., Tamari, T., Sugihara, S., Shima, N., 2022. Characterization of atmospheric tritiated water concentration in the vicinity of the Fukushima Daiichi nuclear power plant. J. Radioanal. Nucl. Chem. https://doi.org/10.1007/s10967-022-08374-2.

Hofschreuder, P., van der Meulen, W., Heeres, P., Slanina, S., 1999. The influence of geometry and draught shields on the performance of passive samplers. J. Environ. Monit. 1, 143–147. https://doi.org/10.1039/a809269i.

Hou, X., 2018. Liquid scintillation counting for determination of radionuclides in environmental and nuclear application. J. Radioanal. Nucl. Chem. 318 (3), 1597–1628. https://doi.org/10.1007/s10967-018-6258-6.

IAEA, 2022. The Database on Nuclear Power Reactors. https://pris.iaea.org/PRIS/home.aspx (accessed 20 June 2022).

Iida, T., Yokoyama, S., Fukuda, H., Ikebe, Y., 1995. A simple passive method of collecting water vapour for environmental tritium monitoring. Radiat. Prot. Dosim. 58, 23–27. https://doi.org/10.1093/oxfordjournals.rpd.a082593.

Jean-Baptiste, P., Fourré, E., Dapoigny, A., Baumier, D., Baglan, N., Alanic, G., 2010. ^{3}He mass spectrometry for very low-level measurement of organic tritium in environmental samples. J. Environ. Radioact. 101, 185–190. https://doi.org/10.1016/j.jenvrad.2009.10.005.

Jean-Baptiste, P., Fontugne, M., Fourré, E., Marang, L., Antonelli, C., Charmasson, S., Siclet, F., 2018. Tritium and radiocarbon levels in the Rhône river delta and along the French Mediterranean coastline. J. Environ. Radioact. 187, 53–64. https://doi.org/10.1016/j.jenvrad.2018.01.031.

Kamath, S., Narayana, B., D'Souza, R., Nayak, R., Mohan, M., Dileep, B., Baburajan, A., Ravi, P., Karunakara, N., 2018. Tritium concentration in ambient air around Kaiga Nuclear Power Plant. Radiat. Prot. Environ. 41, 16. https://doi.org/10.4103/rpe.rpe_20_18.

Kim, D., Croudace, I.W., Warwick, P.E., 2012. The requirement for proper storage of nuclear and related decommissioning samples to safeguard accuracy of tritium data. J. Hazard. Mater. 213–214, 292–298. https://doi.org/10.1016/j.jhazmat.2012.01.094.

Klánová, J., Èupr, P., Kohoutek, J., Harner, T., 2008. Assessing the influence of meteorological parameters on the performance of polyurethane foam-based passive air samplers. Environ. Sci. Technol. 42, 550–555. https://doi.org/10.1021/es072098o.

Ko, Y.G., Kim, C.J., Cho, Y.H., Chung, K.H., Kang, M.J., 2017. Combustion/absorption process for the separation of ^{14}C and ^{3}H in radwastes released from nuclear power plants and their analysis. J. Hazard. Mater. 331, 13–20. https://doi.org/10.1016/j.jhazmat.2017.02.020.

Le Goff, P., Fromm, M., Vichot, L., Badot, P.M., Guétat, P., 2014. Isotopic fractionation of tritium in biological systems. Environ. Int. 65, 116–126. https://doi.org/10.1016/j.envint.2013.12.020.

Morgenstern, U., Stewart, M.K., Stenger, R., 2010. Dating of streamwater using tritium in a post nuclear bomb pulse world: Continuous variation of mean transit time with streamflow. Hydrol. Earth Syst. Sci. 14, 2289–2301. https://doi.org/10.5194/hess-14-2289-2010.

Nie, B., Ni, M., Wei, S., 2017. Individual dose due to radioactivity accidental release from fusion reactor. J. Hazard. Mater. 327, 135–143. https://doi.org/10.1016/j.jhazmat.2016.12.018.

Nie, B., Fang, S., Jiang, M., Wang, L., Ni, M., Zheng, J., Yang, Z., Li, F., 2021. Anthropogenic tritium: Inventory, discharge, environmental behavior and health effects. Renew. Sustain. Energy Rev. 135, 110188 https://doi.org/10.1016/j.rser.2020.110188.

Nie, B., Wu, S., Yang, D., Chen, D., Gu, W., Zhou, W., Yin, J., Wang, D., 2022. Quantitative prediction of dynamic HTO migration behavior in the soil and non-negligible evapotranspiration effect. J. Hazard. Mater. 425, 127772 https://doi.org/10.1016/j.jhazmat.2021.127772.

Nivesse, A.L., Baglan, N., Montavon, G., Péron, O., 2021. New insights into the accessibility of native cellulose to environmental contaminants toward tritium behavior prediction. J. Hazard. Mater. 420, 1–5. https://doi.org/10.1016/j.jhazmat.2021.126619.

Qin, L., Xia, Z., Gu, S., Zhang, D., Bao, G., Han, X., Ma, Y., Deng, K., Liu, J., Zhang, Q., Ma, Z., Yang, G., Liu, W., Liu, G., 2018. A novel atmospheric tritium sampling system. Nucl. Instruments Methods Phys. Res. Sect. A Accel. Spectrometers. Detect. Assoc. Equip. 892, 127–133. https://doi.org/10.1016/j.nima.2017.12.029.

Qin, L., Dai, Z., Xia, Z., Ma, Y., Deng, K., Liu, J., Ma, Z., Zhang, Q., Yang, G., Wei, F., Wu, S., Bao, G., Liu, W., Liu, G., 2019. Evaluation of Dose Derived from HTO for adults in the vicinity of Qinshan nuclear power base. Health Phys. 117, 443–448. https://doi.org/10.1097/HP.0000000000001072.

Querfeld, R., Pasi, A.E., Shozugawa, K., Vockenhuber, C., Synal, H.A., Steier, P., Steinhauser, G., 2019. Radionuclides in surface waters around the damaged Fukushima Daiichi NPP one month after the accident: Evidence of significant tritium release into the environment. Sci. Total Environ. 689, 451–456. https://doi.org/10.1016/j.scitotenv.2019.06.362.

Rauert, C., Schuster, J.K., Eng, A., Harner, T., 2018. Global atmospheric concentrations of brominated and chlorinated flame retardants and organophosphate esters. Environ. Sci. Technol. 52, 2777–2789. https://doi.org/10.1021/acs.est.7b06239.

Salim, F., Górecki, T., 2019. Theory and modelling approaches to passive sampling. Environ. Sci. Process. Impacts 21, 1618–1641. https://doi.org/10.1039/c9em00215d.

Snow, M.A., Feigis, M., Lei, Y.D., Mitchell, C.P.J., Wania, F., 2021. Development, characterization, and testing of a personal passive sampler for measuring inhalation exposure to gaseous elemental mercury. Environ. Int. 146, 106264 https://doi.org/10.1016/j.envint.2020.106264.

Uda, T., Sugiyama, T., Tanaka, M., Munakata, K., Momoshima, N., 2006. Developments of gaseous water, hydrogen and methane sampling system for environmental tritium monitoring. Fusion Eng. Des. 81, 1385–1390. https://doi.org/10.1016/j.fusengdes.2005.08.077.

UNSCEAR, 2017. Sources, effects and risks of ionizing radiation (Annex C): Biological Effects of Selected Integrnal emitters-Tritium. United Nation: New York.

Üzmez, Ö.Ö., Gaga, E.O., Ercan, Ö., Ceylan, Ö., Döğeroğlu, T., 2020. Performance evaluation of a new three-in one diffusive sampler for monitoring NO_2, SO_2 and O_3. Talanta 214, 120829. https://doi.org/10.1016/j.talanta.2020.120829.

Wood, M.J., 1996. Outdoor field evaluation of passive tritiated water vapor samplers at Canadian power reactor sites. Health Phys. 70, 258–267. https://doi.org/10.1097/00004032-199602000-00015.

Wood, M.J., Workman, W.J.G., 1992. Environmental monitoring of tritium in air with passive diffusion samplers. Fusion Technol. 21, 529–535. https://doi.org/10.13182/fst92-a29801.

Zhang, X., Tsurukawa, M., Nakano, T., Lei, Y.D., Wania, F., 2011. Sampling medium side resistance to uptake of semivolatile organic compounds in passive air samplers. Environ. Sci. Technol. 45, 10509–10515. https://doi.org/10.1021/es2032373.

Zhang, X., Brown, T.N., Ansari, A., Yeun, B., Kitaoka, K., Kondo, A., Lei, Y.D., Wania, F., 2013. Effect of wind on the chemical uptake kinetics of a passive air sampler. Environ. Sci. Technol. 47, 7868–7875. https://doi.org/10.1021/es401486f.

Zhang, X., Barnes, J., Lei, Y.D., Wania, F., 2017. Semivolatile Organic Contaminants in the Hawaiian Atmosphere. Environ. Sci. Technol. 51, 11634–11642. https://doi.org/10.1021/acs.est.7b03841.

Zhang, X., Wania, F., 2012. Modeling the uptake of semivolatile organic compounds by passive air samplers: Importance of mass transfer processes within the porous

sampling media. Environ. Sci. Technol. 46, 9563–9570. https://doi.org/10.1021/es302334r.
Zhang, X., Wong, C., Lei, Y.D., Wania, F., 2012a. Influence of sampler configuration on the uptake kinetics of a passive air sampler. Environ. Sci. Technol. 46, 397–403. https://doi.org/10.1021/es203292x.
Zhao, C., Wang, G., Zhang, M., Wang, G., de With, G., Bezhenar, R., Maderich, V., Xia, C., Zhao, B., Jung, K.T., Periáñez, R., Akhir, M.F., Sangmanee, C., Qiao, F., 2021. Transport and dispersion of tritium from the radioactive water of the Fukushima Daiichi nuclear plant. Mar. Pollut. Bull. 169, 112515 https://doi.org/10.1016/j.marpolbul.2021.112515.

Further reading

Liu, Q., Li, L., Zhang, X., Saini, A., Li, W., Hung, H., Hao, C., Li, K., Lee, P., Wentzell, J.J. B., Huo, C., Li, S.M., Harner, T., Liggio, J., 2021. Uncovering global-scale risks from commercial chemicals in air. Nature 600, 456–461. https://doi.org/10.1038/s41586-021-04134-6.
Namieśnik, J., Zabiegała, B., Kot-Wasik, A., Partyka, M., Wasik, A., 2005. Passive sampling and/or extraction techniques in environmental analysis: a review. Anal. Bioanal. Chem. 381, 279–301. https://doi.org/10.1007/s00216-004-2830-8.